

Intrinsic rotation generation in NSTX ohmic H-mode plasmas

This article has been downloaded from IOPscience. Please scroll down to see the full text article.

2013 Nucl. Fusion 53 063012

(<http://iopscience.iop.org/0029-5515/53/6/063012>)

View [the table of contents for this issue](#), or go to the [journal homepage](#) for more

Download details:

IP Address: 198.125.232.176

The article was downloaded on 10/06/2013 at 16:30

Please note that [terms and conditions apply](#).

Intrinsic rotation generation in NSTX ohmic H-mode plasmas

Jong-Kyu Park¹, Ronald E. Bell¹, Stanley M. Kaye¹,
Wayne M. Solomon¹, Benoît P. LeBlanc¹, Ahmed Diallo¹,
Jonathan E. Menard¹, Shigeyuki Kubota² and the NSTX
Research Team¹

¹Princeton Plasma Physics Laboratory, Princeton, NJ 08543, USA

²University of California in Los Angeles, Los Angeles, CA 90095, USA

Received 19 June 2012, accepted for publication 18 April 2013

Published 8 May 2013

Online at stacks.iop.org/NF/53/063012

Abstract

Intrinsic rotation generation was observed and investigated in NSTX ohmic plasmas, by utilizing passive views of charge exchange recombination diagnostics. Focus was placed on ohmic L–H transitions to minimize the effects by other momentum exchange and sources such as the NTV torque by intrinsic error fields. Results indicated that intrinsic rotation generation in the edge is well correlated with ion temperature gradient change, compared with much weaker correlations with electron temperature gradient or density gradient change. This is consistent with a corresponding theory of residual stress, and the measured torque could be directly compared with the theoretical prediction using χ_i as a free parameter. However, an uncertainty on the order of diamagnetic rotation exists in many places across measurement and theory, as will be discussed in detail in this paper.

(Some figures may appear in colour only in the online journal)

1. Introduction

Intrinsic toroidal rotation and torque are important subjects in tokamaks as they are expected to play a dominant role in establishing toroidal rotation in ITER. Toroidal rotation is linked to $\vec{E} \times \vec{B}$ rotation and its shearing rate, which can strongly influence various instabilities from macroscopic scale [1, 2] to microscopic scale [3, 4], and therefore better understanding of intrinsic toroidal rotation can lead to better stability prediction in ITER.

The *intrinsic* toroidal rotation refers to a finite toroidal rotation without any toroidal momentum injection in a tokamak. Obviously, there is no momentum injection in ohmically heated plasmas, but a substantial toroidal rotation has been observed and reported in ohmic L-mode, and more often in ohmic H-mode discharges from many devices, such as COMPASS-D [5], Alcator C-Mod [6–8], DIII-D [9, 10], TCV [11] and ASDEX-U [12]. This paper will add another case from a Spherical Torus, National Spherical Torus eXperiment (NSTX) [13], by utilizing passive views of charge exchange recombination spectroscopy (CHERS).

The intrinsic rotation is often observed to be stronger in H-mode than in L-mode, indicating the relation of the intrinsic rotation to the confined thermal energy, as empirically well known by the W_p/I_p scaling [14], where W_p is the plasma stored energy and I_p is the plasma current. The same trends have been found in discharges with radio frequency (RF) wave

heating, such as ICRF, ECH, and LH (see also [14]) although the possibility of momentum exchange between waves and high energy particles may exist and thus it may not be entirely clear if RF-heated discharges are indeed free from an external toroidal momentum injection.

Even in a truly intrinsic situation, i.e. without any toroidal momentum injection, the momentum exchange across the plasma and with external systems can make the determination of the intrinsic torque from a measured toroidal rotation [15] difficult. Major processes in momentum exchange are the momentum diffusion, and the momentum convection such as the Coriolis pinch [16, 17], and the momentum transport driven by toroidal asymmetry in the magnetic field [18, 19]. Including the intrinsic drive of momentum, these processes are often not easily distinguishable from each other in practice and would require the complete information of the rotation profile evolution with a relevant model for each part.

An innovative method for determining the intrinsic torque was used in DIII-D, using the fact that the momentum diffusion and pinch effects can be minimized if rotation is substantially reduced, and by estimating the required NBI torque to balance against the intrinsic rotation and thus to maintain almost the zero level of rotation [20]. This method, unfortunately, requires balanced NBI beams, which are not commonly available in other devices. In this study on NSTX, the focus was placed on the intrinsic drive of rotation in a short time period across the L–H transition, during which

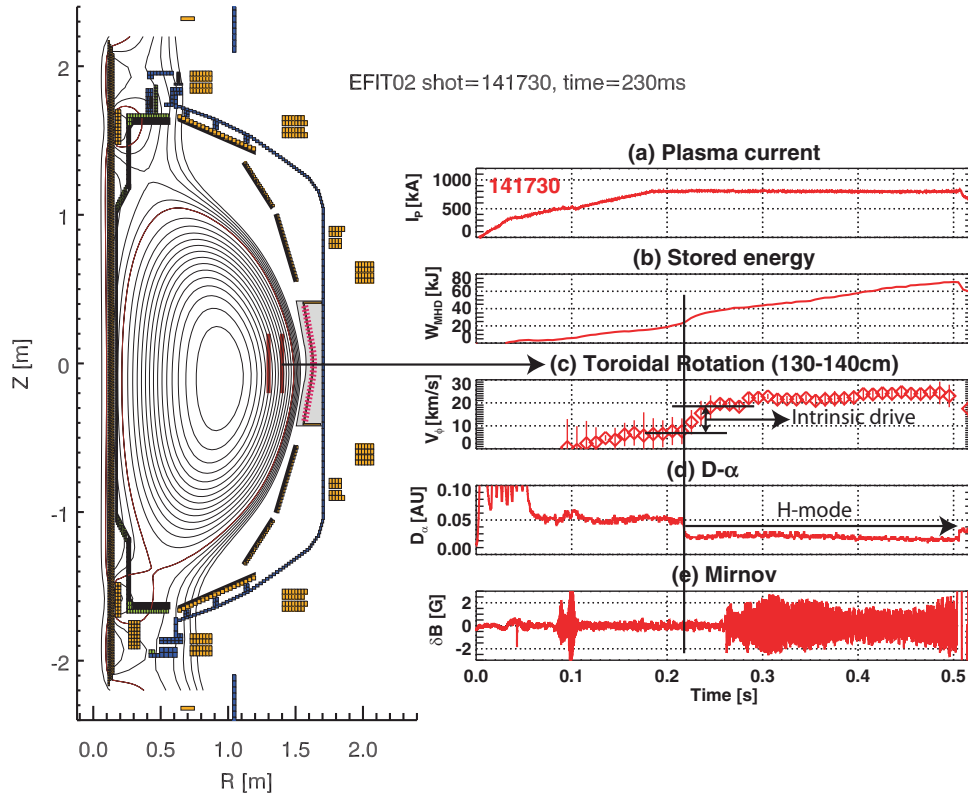


Figure 1. An example of NSTX ohmic H-mode discharge (#141730) with time traces for (a) plasma current, (b) stored energy, (c) toroidal rotation, (d) D_α and (e) Mirnov signal indicating tearing modes later in time. The L–H transition occurred at $t \sim 220$ ms as indicated by the black vertical line. The toroidal rotation in (c) is the average of the edge rotation in $R = 130$ – 140 cm, which was measured by passive views of CHERS. One can see the rapid increase in the toroidal rotation right after the L–H transition.

the momentum diffusion or pinch effects should be ignorable unless the momentum confinement time is comparably short.

Another favourable feature of ohmic plasmas for the study of the intrinsic torque is the weak momentum damping by toroidal asymmetry in the magnetic field. A toroidal asymmetry almost always exists in tokamaks due to intrinsic machine errors and can play a significant role in establishing the rotation profile by neoclassical toroidal viscosity (NTV) torque [19, 21, 22], depending on the level of the toroidal asymmetry and the parametric regime. This *NTV torque by intrinsic error field* itself is a very complicated subject and is not the main focus of this paper. Nonetheless, its effect on our studied cases will be discussed with actual calculations in the appendix, to illustrate the small NTV in ohmic plasmas.

Once the intrinsic torque is separated out from experiments, one can make a comparison with theoretical prediction. One of novel mechanisms predicted in theory is the residual part of Reynolds stress, by the reflection symmetry breaking in the parallel wave vector k_{\parallel} of turbulence [23–25]. This concept can be summarized as a conversion of thermal energy into momentum by drift wave turbulence excited by inhomogeneity in temperature T or density n . So eventually the predicted intrinsic torque is strongly related to ∇T or ∇n , as will be tested in this study. Other mechanisms, such as geometrical up–down asymmetry [26] or charge separation from the polarization drift [27], are ignored, since most of the studied discharges here are up–down symmetric, and the investigated region is near the pedestal where the residual stress is expected to play a major role.

Note that another issue exists in the measurement itself, as most of the diagnostics measure the rotation of impurity ions,

rather than main ions, which therefore should be inferred based on the equilibrium flow balance. The main uncertainty in the flow balance is the poloidal rotation of each species, which should also be inferred unless directly measured. Neoclassical theory is commonly used to estimate the balance between flows and the poloidal rotation, but the uncertainty can be as large as the intrinsic rotation itself, in both measurement and theory, as will be discussed in this paper. This paper is organized as follows. Section 2 will describe the studied NSTX experiments and observations for intrinsic rotation during ohmic L–H transitions, as well as the correlation with the temperature or density gradient. Section 3 will discuss the torque balance and comparisons with a corresponding theory of residual stress, followed by summary and discussion in section 4.

2. Observation for intrinsic rotation and correlation with ion temperature gradient

The increase in toroidal rotation to the co- I_p direction was clearly observed in NSTX ohmic H-mode plasmas, as has been reported in many other devices. Figure 1 shows a typical target plasma and time traces of important plasma parameters in experiments. This is an 800 kA ohmic discharge, with $\kappa \sim 1.9$, $\delta_{\text{ave}} \sim 0.51$, $q_{95} \sim 8.2$, and with almost up–down symmetrical double-null. A few exceptional cases with up–down asymmetry were also studied, but no apparent difference was found in results, indicating that intrinsic rotation drive by up–down asymmetry is not a dominant mechanism in these plasmas and so can be ignored in this study. The shot shown in figure 1 went into the H-mode at $t \sim 220$ ms and the H-mode

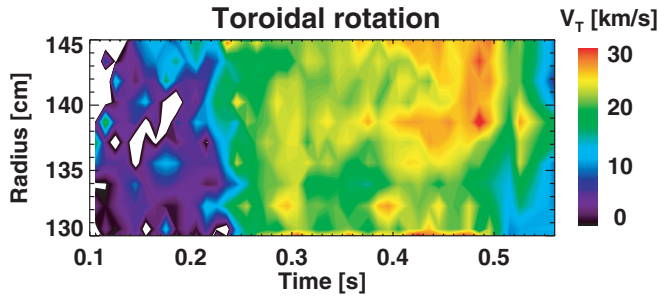


Figure 2. Evolution of carbon toroidal rotation in the edge, measured by passive views of CHERS (#141730). One can see clearly the increase in toroidal rotation by the L–H transition at $t \sim 220$ ms.

was maintained until $t \sim 505$ ms as indicated by the D_α signal and also as can be seen in the increase in stored thermal energy. Toroidal rotation measured in the edge showed fairly rapid increase up to 10 km s^{-1} through the L–H transition, and became almost steady afterwards.

The steady rotation but the continuous increase in thermal energy, at about ~ 30 ms after the L–H transition seems inconsistent with what is implied from the W_p/I_p scaling. However, this is because other effects can eventually come into a play later in the discharge. For instance, in these ohmic H-modes, a tearing mode, as shown by the Mirnov signal in figure 1, might cause a damping against the momentum supply by intrinsic torque. A low torque plasma is better for the study of the intrinsic rotation, but may be vulnerable to MHD modes like tearing modes, which can give an additional momentum transport associated with the modes and further complicate the analysis. Also, the momentum inward pinch can transfer the intrinsic torque in the edge to the core until a balance is reached against the momentum outward diffusion. These momentum exchange effects can be minimized by reducing the measurement time period around the L–H transition, as will be discussed in section 3. Also, normally in this short time period, MHD modes do not appear because the L–H transition with ohmic heating alone may become more difficult when a MHD mode exists in the first place.

In principle, momentum exchange effects can be studied together with the intrinsic torque if profile evolution is fairly well resolved in space and time. This is often limited in the measurement of toroidal rotation without NBI, as is the case in our study. We used passive views of CHERS, which measures the background C^{5+} ions and gives their local toroidal rotation and ion temperature by inverting line-integrated values of 39 sightlines [28]. Because the emissivity for those background ions is not strong enough in the core, the reliability of measurement is limited to the edge region. Comparing the information from passive CHERS with active CHERS in different shots with NBI blips, one can find good agreement in the edge, $R = 130\text{--}145$ cm, or equivalently $\rho = \sqrt{\psi_N} = 0.64\text{--}0.95$.

Figure 2 shows an example of the passive CHERS measurement for toroidal rotation, in the edge $R = 130\text{--}145$ cm as a function of time. The H-mode was achieved and maintained at $t > 220$ ms in this discharge, as shown in figure 1, and one can see the apparent increase in toroidal rotation in the H-mode phase. As introduced already, one of the goals in this study is to investigate any possible correlation

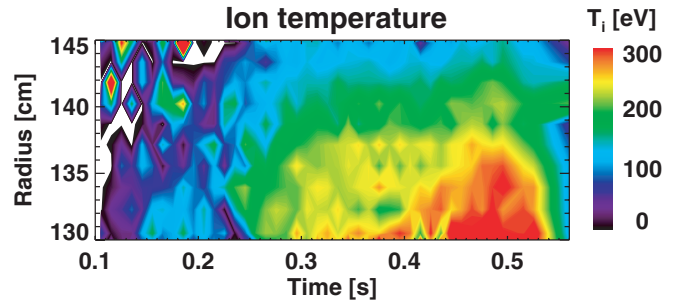


Figure 3. Evolution of ion temperature in the edge, measured by passive views of CHERS (#141730). One can see also the clear increase in ion temperature by the L–H transition at $t \sim 220$ ms, but there is the difference in the spatial profile compared with the toroidal rotation in figure 2.

with temperature or density gradient, and thus ion temperature profile evolution is also investigated using the passive CHERS as shown in figure 3. An interesting feature can be unveiled if one compares figures 2 and 3, and notices that their peak values are located differently in space, indicating the possibility of correlation between rotation and ion temperature gradient, rather than ion temperature itself.

The information of the profile gradient is harder to resolve than the profile itself due to various error sources in measurement and inversion of passive data. In particular, noises upon the overall envelope should be eliminated by smooth fitting to estimate the profile gradient. We selected three spatial points at $R \sim 132$ cm, $R \sim 136$ cm and $R \gtrsim 140$ cm, and obtained the amplitude and the gradient by taking a spatial average over ~ 4 cm. Magnetic equilibria in the studied discharges are all quite similar and the selected radial positions correspond to $0.64 < \rho < 0.72$, $0.72 < \rho < 0.80$ and $\rho > 0.80$, respectively. Estimated errors are all maintained, from the emissivity, to the inversion, to the profile smoothing for the gradient information, and are shown in all of the correlation results presented in this paper. Regarding the electron density and temperature information, other radial positions deeper in the core can also be studied since multi-point Thomson scattering diagnostics provides reliable measurements from the outboard to the inboard area. However, just for comparison, only the same spatial points, $R \sim 132$ cm, $R \sim 136$ cm and $R \gtrsim 140$ cm, were selected and averaged.

An example of the achieved profiles is shown in figure 4. It shows the edge profile evolution of toroidal rotation, ion temperature and electron density at three different times in L-mode ($t = 165, 175, 185$ ms) and four different times in H-mode ($t = 195, 205, 215, 225$ ms). One can see very rapid changes in toroidal rotation $V \equiv V_\phi$ and ion temperature T_i profiles only through the L–H transition, compared with electron density n_e profiles. Moreover, the greatest change in V occurs at $R < 1.42$ m, which is deeper in the core than the density pedestal. In fact, one can see that the increase in n_e is largely driven by the pedestal development at $R > 1.42$ m, while T_i increases along with a broader gradient increase which can be correlated with the increase in V . Note that the profiles in figure 4 are only for the edge region far from the core and that the n_e profiles exhibit a dip on the top of the pedestal shortly after the L–H transition. The T_e profiles

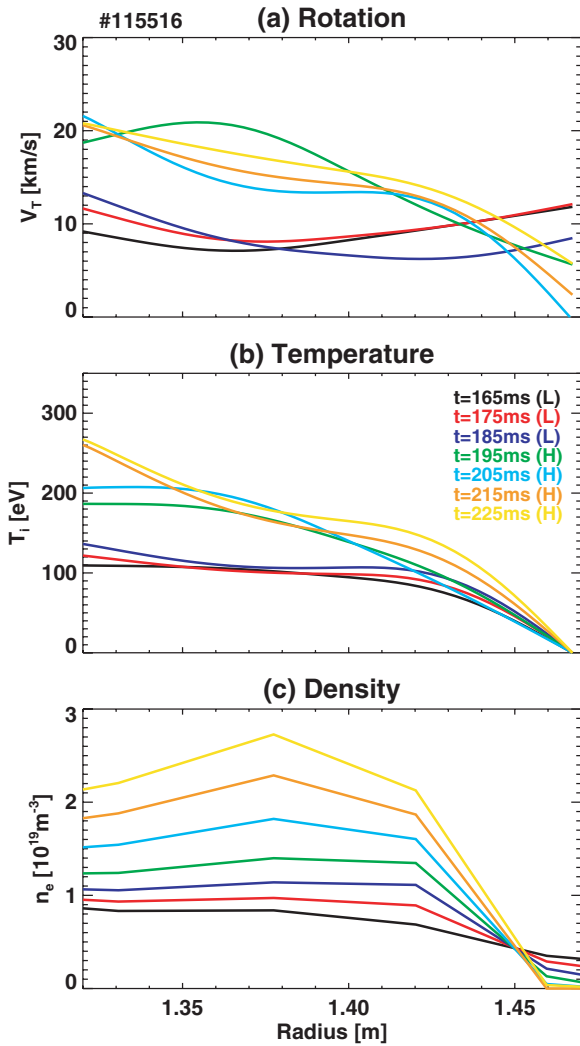


Figure 4. Edge profiles of rotation, temperature, and density after the smoothed fits that are necessary to take the gradient information. Note the separatrix is located at $R = 1.46$ m, and the magnetic axis $R \sim 1.0$ m is far from the left. Passive CHERS becomes unreliable with larger errors in $R < 1.30$ m. The time resolution is limited by $\Delta t \sim 10$ ms. One can see clearly the rapid change in toroidal rotation and ion temperature through the L–H transition ($t = 185$ ms $\rightarrow t = 195$ ms).

are not shown here for simplicity, but their gradient increase is quite similar to the n_e . The n_i profiles will be not discussed in this paper since the direct measurements are not available, but it is found that $n_i \sim n_e$ within 10% when checked from NBI blips, assuming the active CHERS measures the dominant low Z impurity. The NBI blips were used via several times to diagnose the agreement between passive CHERS and active CHERS, but those data are not applicable to this study due to the strong momentum drive by NBIs. Note a very large change in V occurs within 10 ms during the L–H transition, but unfortunately, 10 ms was the time resolution used in these experiments and so the detailed dynamics in such a short time period could not be investigated.

Using the profile information, correlation studies were carried out over ~ 10 ohmic H-mode discharges in NSTX 2005–2011 operation. At the selected radial positions in each shot, the change in toroidal rotation ΔV was compared with the change in temperature and density gradient $\Delta(dT/d\psi)$ and $\Delta(T/n)(dn/d\psi)$ in 10 ms during the L–H transition. The

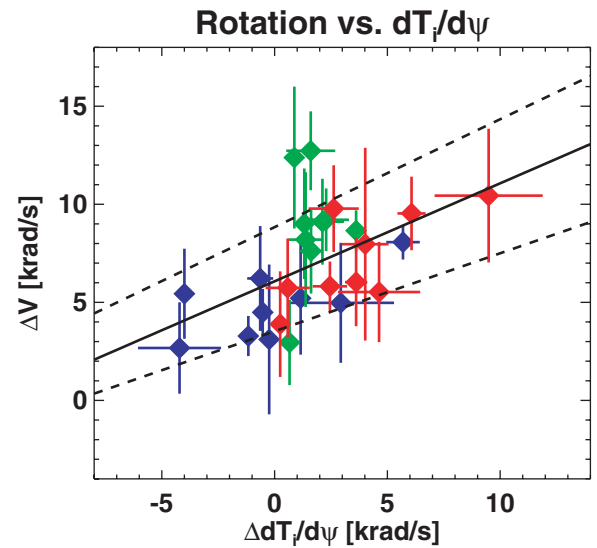


Figure 5. Correlation between the measured changes in carbon toroidal rotation and ion temperature gradient through the L–H transition. One can find $\Delta V_{\text{Ex}} = C_z \Delta V_d$ with $C_z \approx 0.50$ on average with an offset $\sim 5 \text{ km s}^{-1}$. Here the different locations are coded with different colours; the blue colors are for $0.64 < \rho < 0.72$, the green colors for $0.72 < \rho < 0.80$ and the red colours for $\rho > 0.80$. The same colour codes are applied to subsequent figures 5, 6 and 8–10. There is a reasonable positive correlation compared with figure 6.

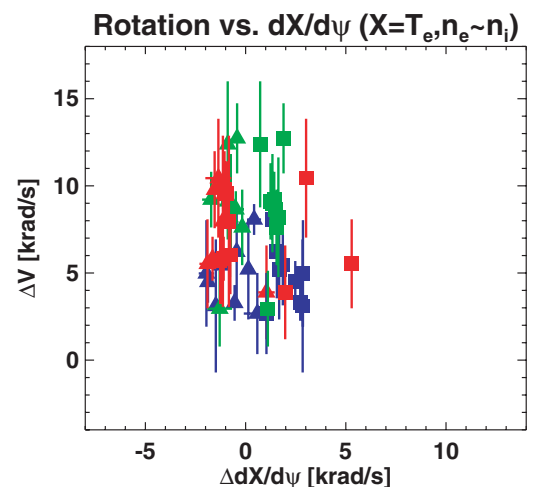


Figure 6. Correlation between the measured changes in carbon toroidal rotation and electron temperature (square) and density (triangle) through the L–H transition. There is no apparent correlation found. Note for the electron density, $dX/d\psi \equiv (T_e/n_e)dn_e/d\psi$.

reason why the change Δ is measured in a short time period is also to minimize other momentum exchange effects, which will be further discussed later along with torque balance issues.

As the possibility was discussed from the profile information, figure 4, the best correlation was found with the ion temperature gradient, as shown in figure 5, whereas correlations with the electron temperature and density gradients are much weaker, as shown in figure 6. Here the different colours indicate the different spatial locations of measured data. The blue colours are for $0.64 < \rho < 0.72$, the green colours for $0.72 < \rho < 0.80$ and the red colours for $\rho > 0.80$. All together, it was found that

$$\Delta V_{\text{Ex}} = C_z \Delta V_d \quad (1)$$

with $C_z \approx 0.50$, where a diamagnetic-like speed V_d is defined as

$$V_d \equiv -RdT_i/d\psi, \quad (2)$$

where R is the major radius of the location. This is a convenient quantity from the experimental point of view, since $dT/d\psi$ becomes in units of rad s^{-1} when units of T (eV) and the poloidal flux function $\psi = \psi_{\text{pol}} (\text{Wb})/2\pi$ are used. The minus sign just indicates the poloidal flux function is defined to be increased towards the edge and so typically $dT/d\psi < 0$ and will be omitted unless it is needed.

One may notice that an offset exists in the correlation with the ion temperature gradient, in figure 5, of up to 5 km s^{-1} within error bars. An offset was also found in recent DIII-D results [20]. The offset means that the toroidal rotation can increase even when the ion temperature gradient does not increase. Note that the ion temperature gradient was even reduced in several occasions, especially for $0.64 < \rho < 0.72$ (blue), but it is just because that the ion temperature gradient can be steeper in L-mode when the location approaches the core region. Even in these cases the rotation increases slightly, and this observation led us to investigate any possible correlation with the direct change in the temperature ΔT since the ion temperature itself always increases during L–H transition. However, a correlation was very poor overall, indicating a mechanism associated with the temperature itself, e.g. the direct momentum transport by ion orbit losses, may be involved depending on the location but should not be the main mechanism driving the increase in the rotation in our cases.

The correlation found with the ion temperature gradient is consistent with the prediction of residual-stress theory. Before making a comparison, however, it is necessary to discuss the difference between the measured *impurity rotation* V_z and the *main ion rotation* V_i . Considering the flow balance for each species [29]

$$V_s \cdot \nabla \phi = - \left(\frac{d\Phi}{d\psi} + \frac{1}{Z_s e n_s} \frac{dP_s}{d\psi} - q V_s \cdot \nabla \theta \right), \quad (3)$$

where the contribution from the poloidal rotation is $q V_s \cdot \nabla \theta = (I/R^2)(V_{s\theta}/B_\theta)$ with $I = RB_\phi$. The difference in toroidal rotation between V_z and V_i is given by

$$V_i \cdot \nabla \phi - V_z \cdot \nabla \phi = - \left(\frac{1}{en_i} \frac{dP_i}{d\psi} - \frac{1}{Zen_z} \frac{dP_z}{d\psi} \right) + \frac{I}{R^2} \left(\frac{V_{i\theta}}{B_\theta} - \frac{V_{z\theta}}{B_\theta} \right). \quad (4)$$

The impurity diamagnetic rotation ($dP_z/d\psi$) can be ignored in most of the cases, so the difference becomes the difference in the poloidal rotation in addition to the ion diamagnetic rotation ($dP_i/d\psi$). One way to evaluate the poloidal rotation, when it is not directly measured, and thus to obtain the difference in the toroidal rotation using equation (4), is to use the neoclassical theory. A few cases were tested with TRANSP and NCLASS [30, 31] by assuming $Z_{\text{eff}} \sim 1.5$ based on the shot data with NBI blips, as an example is shown in figure 7 at a time slice right after the L–H transition. One can see from figure 7 a significant difference in the toroidal rotation of two species, up to a factor of 2.

In principle, one can run NCLASS for every case to find out the neoclassical prediction for the main ion rotation.

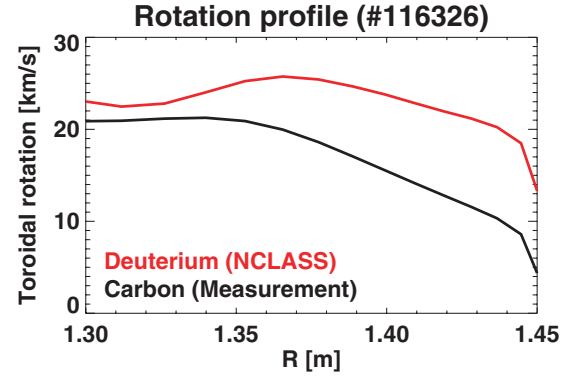


Figure 7. NCLASS prediction for the main ion toroidal rotation using the measured impurity toroidal rotation as an example (#116326 at $t = 195$ ms). $Z_{\text{eff}} = 1.5$ is assumed.

Many assumptions should however be needed, such as carbon and impurity density profiles, and even the available data are only reliable in the limited edge region. Also, although the neoclassical prediction has provided a reliable guidance for the poloidal rotation [32, 33], recent studies are indicating the conventional neoclassical estimation for the poloidal rotation should be modified or may be incorrect depending on parameters and configurations. For instance, Alcator C-Mod experiments implied the possibility of a strong change in the poloidal rotation by $\vec{E} \times \vec{B}$ [34], and DIII-D experiments showed the discrepancy between theory and direct measurements in the banana regime [35]. Moreover, NSTX studies showed the measured poloidal rotation is much smaller than NCLASS or GTC-NEO [36] simulations especially in the edge [28]. If one uses this NSTX empirical observation and neglects the poloidal rotation, the difference between the main ion and carbon rotation becomes as large as the diamagnetic rotation of the main ions. Of course the empirical observation was about impurity ions and does not imply that the main ion poloidal rotation can also be neglected. In fact, it can be as large as the diamagnetic term and give the typical simplification $V_i \cdot \nabla \phi = V_z \cdot \nabla \phi$, based on the assumption of the parallel flow balance. The range of the difference in toroidal rotation then can be expected to be

$$0 \lesssim V_i \cdot \nabla \phi - V_z \cdot \nabla \phi \lesssim - \frac{1}{en_i} \frac{dP_i}{d\psi}. \quad (5)$$

The uncertainty comparable to the ion diamagnetic rotation, which in fact always exists in the toroidal rotation measurement, would be ignorable for fast rotating cases with NBIs, but would be significant when the intrinsic rotation is considered. Combining equation (5) with equation (1), the change in the toroidal rotation of main ions becomes $C_z \Delta V_d \lesssim \Delta V_{\text{Ex}} \lesssim (1 + C_z) \Delta V_d$, where the measured value from carbon ions is $C_z \approx 0.50$, which is less than the diamagnetic rotation. Here the density gradient change, $(T/n)dn/d\psi$, is ignored for simplicity as it gives only $\sim 10\%$ difference for correlation. Figure 8 shows the correlation when the difference by diamagnetic rotation is fully taken into account.

One can see a significant change in the correlation, which is better aligned of course due to the self-additive term by $dT/d\psi$. The actual answer is likely between figures 5

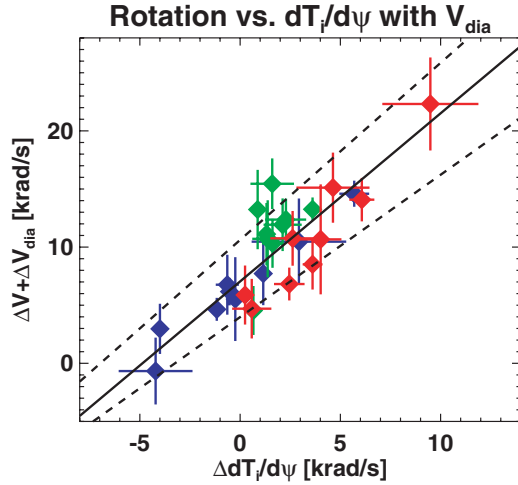


Figure 8. Revised correlation with ion temperature gradient for the main ion rotation, which is calculated by neoclassical flow balance ignoring the poloidal rotation [28] and impurity pressure. As a result, the toroidal rotation change is increased by the diamagnetic rotation change.

and 8. One must be careful to interpret the contribution of the diamagnetic rotation. This is not an intrinsic drive of rotation, but just an offset that one must consider to correct an imperfect measurement. If there is no intrinsic rotation generation, this diamagnetic rotation will be compensated by the change in $\vec{E} \times \vec{B}$ and the net toroidal torque and the rotation generation should not be observed. Now a question is how much the turbulent intrinsic drive can contribute to the observed toroidal rotation within this neoclassical uncertainty. The next section will discuss a corresponding theoretical prediction and the comparison with our measurements.

3. Torque balance and comparison with theory

The increase in the toroidal rotation without an external torque is driven by intrinsic toroidal torque. The intrinsic torque is the more fundamental mechanism and the rotation is the consequence of the torque balance between the momentum exchange. For comparison with experiments, consider the torque balance in a cylindrical limit,

$$\frac{\partial(MnRV)}{\partial t} = T_{\text{input}} - \nabla \cdot \Pi_{r\phi}^{3D} - \nabla \cdot \Pi_{r\phi}, \quad (6)$$

where

$$\Pi_{r\phi} = -MnR \left(\chi_\phi \frac{dV}{dr} - V_{\text{pinch}} V \right) + \Pi_{r\phi}^{\text{ex}}. \quad (7)$$

Obviously, the input torque is zero, i.e. $T_{\text{input}} = 0$, in ohmic plasmas. The torque by 3D field $\nabla \cdot \Pi_{r\phi}^{3D}$ includes the resonant electromagnetic torque at the rational surfaces by tearing or locked modes and also the NTV torque [19, 21, 22] by broken axisymmetry. The NTV torque almost always exists in tokamaks due to intrinsic asymmetry in the magnetic field, and it is not ignorable especially for a low torque plasma. This *NTV torque by intrinsic error field* is, however, small in ohmic plasmas, due to the low pressure and the high collisionality, and can be ignored in this study, i.e. $\nabla \cdot \Pi_{r\phi}^{3D} = 0$. Actual modelling is presented in the appendix.

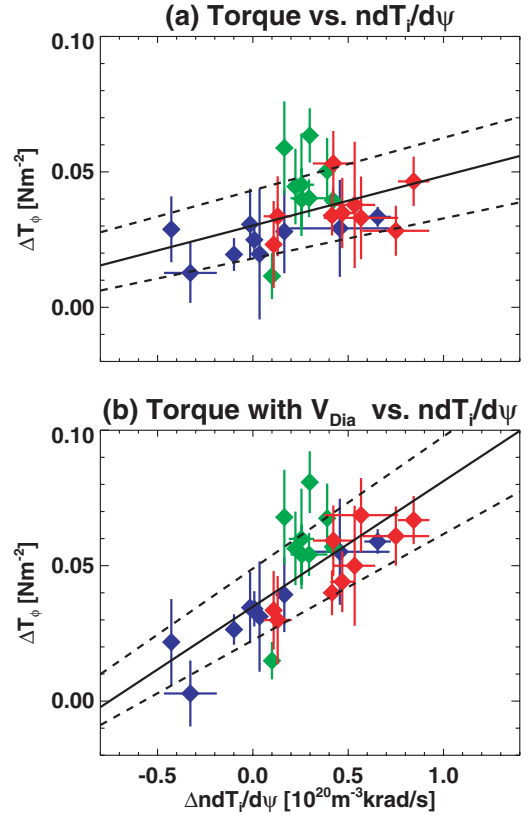


Figure 9. Correlation between measured torque density change and ion temperature gradient change (with the density multiplied) through the L–H transition. (a) assumes $V_1 \cdot \nabla\phi - V_z \cdot \nabla\phi = 0$ and (b) assumes $V_1 \cdot \nabla\phi - V_z \cdot \nabla\phi = -(1/en)(dP/d\psi)$.

Now assuming $\nabla \cdot (MnR\chi_\phi dV/dr - MnRV_{\text{pinch}}V) = -MnRV/\tau_\phi$ and the momentum confinement time $\tau_\phi \gg 10$ ms based on previous NSTX momentum transport studies [15], dominant terms through the L–H transition within $\Delta t \sim 10$ ms $\ll \tau_\phi$ are

$$\frac{\Delta(MnRV)}{\Delta t} \approx -\nabla \cdot \Pi_{r\phi}^{\text{ex}} \equiv T_\phi^{\text{ex}}. \quad (8)$$

Therefore, the increase in the toroidal rotation in these ohmic experiments can be considered as the drive by a pure intrinsic torque change. Note that the assumption $\tau_\phi \gg 10$ ms may not be merely applicable to ohmic plasmas, and also that the momentum exchange may be locally very different, but their effects are minimized by taking the measurement limit ~ 10 ms in our study. One can estimate the intrinsic torque with equation (8) from measurements, and can study the correlation with the ion temperature change, as shown in figure 9. Here the density is multiplied additionally as the inertial effect exists between the rotation change and the exerted torque. It should be distinguished from the pressure gradient, which includes the density gradient that is not relevant for the intrinsic torque in either experiment or theory.

Including the correlation with the diamagnetic rotation, it is found

$$T_\phi^{\text{ex}} = C_{\text{ex}} n R V_d, \quad (9)$$

where $C_{\text{ex}} \approx 3.0 \times 10^{-2}(1 + C_z)$ when units n (10^{20} m^{-3}) and V_d (km s^{-1}) are used. Here C_z represents the measurements by impurity ions and 1 represents the uncertainty that is as large as the diamagnetic rotation.

The correlation with $V_d \equiv R dT_i/d\psi$ implies the process of intrinsic rotation drive is essentially associated with the ion-temperature-gradient (ITG) driven mode, as has been proposed theoretically [23, 24] and has been found numerically in GTS simulation [37]. These predictions were also demonstrated experimentally in Alcator C-Mod [38]. Our study suggests that ITG is also possibly a dominant instability, driving turbulence and intrinsic torque in NSTX ohmic H-mode plasmas, over trapped-electron mode (TEM) or electron-temperature-gradient (ETG) driven mode. If TEM or ETG were not negligible, a correlation with electron density or temperature would be pronounced, as found in the study for ASDEX-U with GS simulation [12] and numerically in GTS simulation [39]. When ITG is dominant and if $\vec{E} \times \vec{B}$ shearing rate balances the entropy production from ITG in a stationary state, one can estimate the residual stress and the intrinsic flow in a stationary state using the $\vec{E} \times \vec{B}$ shearing rate. Diamond obtained the residual stress as [24]

$$\Pi_{r||}^{rs} = -MnR \left[\rho_* \chi_i \frac{L_s}{2c_s} \left(\frac{\nabla T}{T} \right)^2 v_{\text{thi}}^2 \right], \quad (10)$$

where the normalized ion sound Larmor radius $\rho_* = \rho_s/a$, ion sound speed $c_s = \sqrt{T_e/M_i}$, shear length $L_s^{-1} = \hat{s}/qR$, ion diffusivity χ_i , and thermal ion speed $v_{\text{thi}} = \sqrt{T_i/M_i}$. Ignoring other spatial variations and higher order spatial temperature variations than T' , and taking a cylindrical approximation, i.e. $\hat{\phi} \sim \hat{b}$, one can obtain the theoretical intrinsic torque density as

$$T_\phi^{rs} = \frac{MnR\chi_i}{2\hat{s}L_T^2} V_d. \quad (11)$$

Then this becomes consistent with observation as they both are correlated with the ion temperature gradient $V_d \propto \nabla T$. Note it is assumed in the theory that L_T is almost fixed, and thus from the experiment it is also assumed that $L_T \sim 10$ cm on average which is the width of the temperature pedestal, although there is additional dependence on the temperature gradient in L_T . For deuterium ions and adopting previous units again, one has

$$T_\phi^{rs} = C_{rs} n R V_d, \quad (12)$$

where $C_{rs} = 1.7 \times 10^{-4} \hat{s} (\chi_i/L_T^2)$ for the deuterium main ions. Using equation (12), the theory and experiment can be quantitatively compared using χ_i as a free parameter for different locations, as shown in figure 10. The variation in χ_i is quite large, $0.4 \text{ m}^2 \text{ s}^{-1} < \chi_i < 6.1 \text{ m}^2 \text{ s}^{-1}$, but this range is similar to what was found from the previous momentum studies in NSTX L-modes [40]. Also, one can see that the highest χ_i can be found in the middle location, at $0.72 < \rho < 0.80$ (green), and this is interestingly consistent with the TRANSP simulation in [40] for L-modes. Of course the assumptions of constant χ_i and L_T may be very crude and especially the higher order temperature dependence can be involved, but it will be quite challenging in the future if the higher order temperature gradients need to be resolved from experiments.

The prediction of toroidal rotation by intrinsic torque is another important issue, but is not straightforward even if the intrinsic torque is well predicted. This is beyond the scope

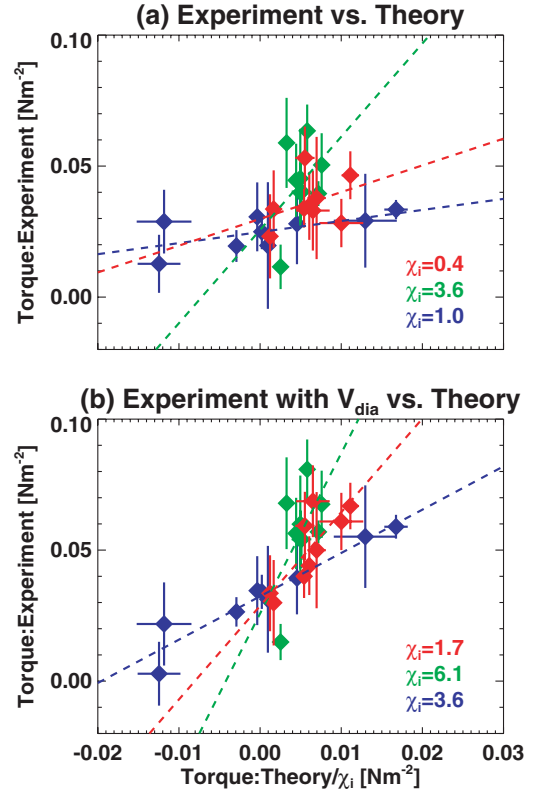


Figure 10. Comparison between residual-stress theory prediction and measurement for torque density, using χ_i ($\text{m}^2 \text{ s}^{-1}$) as a free parameter. (a) assumes $V_i \cdot \nabla \phi - V_z \cdot \nabla \phi = 0$ and (b) assumes $V_i \cdot \nabla \phi - V_z \cdot \nabla \phi = -(1/en)(dP/d\psi)$. From theory, higher order temperature variations than T' and toroidal effects are ignored.

of this paper, but it is interesting to consider the consequence of the theory, equation (10). When there is no other torque than the Reynolds stress term in equation (6), one can use $-\chi_\phi^{\text{eff}} \langle V_\phi \rangle' + \Pi_{r\phi}^{rs} = 0$ in a stationary state. Again ignoring other variations and high order temperature variation, one can integrate it and obtain

$$\frac{\langle V_\phi \rangle}{v_{\text{thi}}} \cong \frac{1}{2} \rho_* \frac{\chi_i}{\chi_\phi^{\text{eff}}} \frac{L_s}{L_T} \sqrt{\frac{T_i}{T_e}}, \quad (13)$$

as obtained by Kosuga [41]. Using $\rho_* = \sqrt{T_e/M_i}/(eB/M_i)/a$, $v_{\text{thi}} = \sqrt{T_i/M_i}$, $L_s = qR/\hat{s}$, and $(1/eB_\theta)dT/dr = R dT/d\psi$, one can see that the equation can be simplified as

$$\langle V_\phi \rangle \cong \frac{1}{2\hat{s}\text{Pr}} V_d, \quad (14)$$

where $\text{Pr} \equiv \chi_\phi^{\text{eff}}/\chi_i$. If Pr is an order of unity, $\text{Pr} \sim 1$, the predicted rotation is possibly much less than the diamagnetic rotation $\sim V_d$. This theoretical prediction is highly unfavourable for tokamaks and it will even be difficult to resolve it in experiments due to the neoclassical uncertainties as discussed in the previous section. If a faster toroidal rotation than a diamagnetic level is desired to avoid various instabilities, a small $\text{Pr} < 1/(2\hat{s})$ is required or otherwise another torque driver will be necessary.

4. Summary and discussion

This paper reported an investigation of intrinsic rotation in NSTX ohmic H-mode plasmas and a comparison with a

corresponding theory of residual stress. Results and issues can be summarized as follows.

- (1) Experimentally, the increase in toroidal rotation, by $\sim 10 \text{ km s}^{-1}$ in the co- I_p direction, was clearly observed during the L–H transition without any external toroidal momentum injection.
- (2) Passive views of CHERS provided essential measurements in the edge region and indicated the best correlation between the increase in toroidal rotation and the ion temperature gradient change, as $\Delta V_{\text{Ex}} = C_z \Delta V_d$, equation (1).
- (3) However, the difference between impurity ions and main ions should be considered. In NSTX, the poloidal rotation may be ignorable and then the flow balance indicated $\Delta V_{\text{Ex}} = (1 + C_z) \Delta V_d$. The neoclassical uncertainties, represented by the order of unity 1 is as large as measured intrinsic rotation and so resolution of the rotational difference between species will be equally important.
- (4) The intrinsic rotation measurement would not guarantee the intrinsic torque measurement, so other torque sources should be carefully considered. These experiments are relatively free from the momentum diffusion, pinch, and NTV damping effects and so relate pure intrinsic torque as $T_\phi^{\text{ex}} = C_{\text{ex}} n R V_d$, equation (9).
- (5) A theory based on residual stress driven by ITG can be simplified as $T_\phi^{rs} = C_{rs} n R V_d$, equation (12), and a good comparison could be made using χ_i as a free parameter.
- (6) However, there are a couple of important issues. First, all of the discussions in this paper are based on a large-aspect-ratio geometry, which may not be so relevant in a spherical torus, and toroidal effects should be taken into account in the future.
- (7) A more important issue is that the full theory predicts the residual stress including $(\nabla T)^2$ and so the torque density involves higher order temperature-gradient dependence, such as $(T')^2$ and T'' . These experiments showed only the correlation with T' , but the resolution in measurements was insufficient to resolve higher order gradients that may be embedded in our free parameter χ_i . A very high spatial resolution in measurements will be challenging without NBI, but seems necessary to resolve the higher order dependence.
- (8) The determination of rotation is a different issue since it additionally requires the information of momentum diffusion and pinch. The corresponding theory predicts $V \cong (1/2\hat{s}\text{Pr})V_d$, which is less than or equal to the diamagnetic level. A small Pr is required or other momentum sources seem necessary to achieve the rotation higher than the diamagnetic rotation.

In future work, it will also be important to consider how the intrinsic toroidal rotation can modify $\vec{E} \times \vec{B}$ rotation, which is the ultimate target in the study of the intrinsic rotation. This part in fact constructs the closed loop among $\vec{E} \times \vec{B}$, the intrinsic torque, and the toroidal rotation. Note that the presented theory of the residual stress begins with $\vec{E} \times \vec{B}$ and assumes the intrinsic flow as the next order. It will be desirable to remove this assumption and incorporate other novel mechanisms of intrinsic torque and rotation together

since all of the pieces involved in the determination of intrinsic rotation may be in a similar order of diamagnetic rotation.

Acknowledgments

We would like to acknowledge useful discussions with Y. Ren, W. Guttenfelder, W.X. Wang, S. Ku and J.A. Krommes on this topic. Also we thank R.G. Andre, C.A. Ludesch-Furth, S.P. Gerhardt for helping TRANSP and NCLASS simulations. This work was supported by DOE contract DE-AC02-09CH11466 (PPPL).

Appendix. Intrinsic NTV torque in NSTX ohmic H-mode

In this appendix, a calculation of torque by intrinsic error field in NSTX will be presented. An intrinsic error field almost always exists in tokamaks due to imperfect axisymmetry and can induce a toroidal torque by non-ambipolar momentum transport. This NTV torque by intrinsic error field can be important in low torque and slowly rotating plasmas, depending on the level of error field and the transport regime.

In NSTX, there are two well-known error fields; the distortion of the centerstack and the non-circularity of PF5 coils. The developed models for both sources have been well validated in previous studies [42, 43] and so they are used to calculate non-axisymmetric variation in the field strength including ideal plasma response. The result for $n = 1$ δB calculated by the ideal perturbed equilibrium code (IPEC) [44] is shown in figure 11. One can see clearly the effects of large error field at the inboard side due to the centerstack distortion, as well as small deviations at the outboard side due to PF5 coil errors [42, 43]. In fact $n = 3$ components are larger than $n = 1$ in PF5 coil errors, but can be ignored compared with the large centerstack distortion in ohmic plasmas and were even corrected by $n = 3$ error field correction (EFC) coils in a few cases.

Using the IPEC δB , a combined NTV formulation was used [22] to calculate the intrinsic NTV torque as this method has been validated in many cases within an order of magnitude [43, 45–47]. The result, figure 12 shows that the NTV torque by intrinsic error field is much less than the measured intrinsic torque. Therefore, the NTV torque by intrinsic error field is neglected in the paper, but note that this should not be generalized to other studies. In fact, two primary reasons of low NTV torque here are the low pressure and the high collisionality in ohmic plasmas. The low pressure reduces the Lagrangian variation in the field strength as well as the plasma response, and the high collisionality reduces the non-ambipolar transport in the $1/\nu$ regime. Considering the NTV torque is proportional to $(\delta B)^2$, one can easily find that $\nabla \cdot \Pi_{r\phi}^{3D}$ can increase very rapidly along the temperature [22]. That is, the NTV torque by intrinsic error field can be important when a high confinement with high temperature is targeted with a low external torque, as is the case in ITER. In ITER, the NTV torque by applied 3D field will also be very important if the 3D field techniques are utilized to improve various MHD instabilities, and should be taken into account together in the prediction of toroidal rotation.

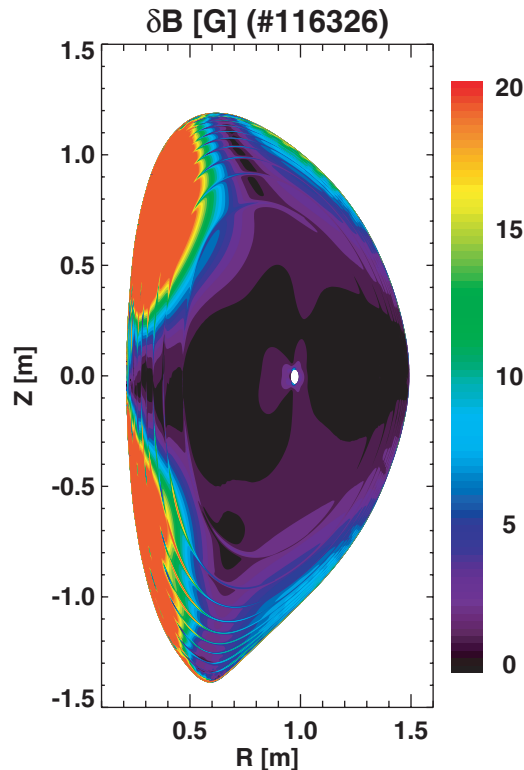


Figure 11. An example of Lagrangian variation in the field strength δB (#116326 at $t = 195$ ms), calculated by IPEC, using the $n = 1$ intrinsic error field model in NSTX. One can see clearly the large error field at the inboard side by centerstack distortion, and the small error at the outboard side by non-circular PF coils.

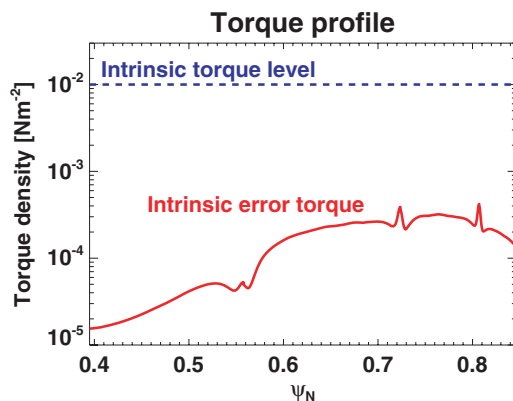


Figure 12. Calculated torque density profile produced by intrinsic error field, using IPEC δB and combined NTV formula. One can see the NTV torque by intrinsic error field, which is denoted by *intrinsic error torque* (red), is small and can be ignored, compared with the measured *intrinsic torque* (blue), as typical in low temperature ohmic plasmas.

References

- [1] Strait E.J., Taylor T.S., Turnbull A.D., Ferron J.R., Lao L.L., Rice B., Sauter O., Thompson S.J. and Wróblewski D. 1995 *Phys. Rev. Lett.* **74** 2483
- [2] Sabbagh S.A., Bell R.E., Menard J.E., Gates D.A., Sontag A.C., Bialek J.M., LeBlanc B.P., Levinton F.M., Tritz K. and Yuh H. 2006 *Phys. Rev. Lett.* **97** 045004
- [3] Burrell K.H. 1997 *Phys. Plasmas* **4** 1499
- [4] Kaye S.M. et al 2007 *Phys. Rev. Lett.* **98** 175002
- [5] Coffey I.H. et al 1996 *Proc. 11th Colloquium on UV and X-Ray Spectroscopy of Astrophysical and Laboratory Plasmas* (Universal Academy, Nagoya, Japan, 1996) (Frontiers Science Series) vol 15
- [6] Rice J., Bonoli P., Goetz J., Greenwald M., Hutchinson I., Marmor E., Porkolab M., Wolfe S., Wukitch S. and Chang C. 1999 *Nucl. Fusion* **39** 1175
- [7] Hutchinson I.H., Rice J.E., Granetz R.S. and Snipes J.A. 2000 *Phys. Rev. Lett.* **84** 3330
- [8] Rice J. et al 2000 *Phys. Plasmas* **7** 1825
- [9] deGrassie J.S., Burrell K.H., Baylor L.R., Houlberg W. and Lohr J. 2004 *Phys. Plasmas* **11** 4323
- [10] deGrassie J.S., Rice J.E., Burrell K.H., Groebner R.J. and Solomon W.M. 2007 *Phys. Plasmas* **14** 056115
- [11] Scarabosio A., Bortolon A., Duval B.P., Karpushov A. and Pochelon A. 2006 *Plasma Phys. Control. Fusion* **48** 663
- [12] Angioni C. et al and the ASDEX Upgrade Team 2011 *Phys. Rev. Lett.* **107** 215003
- [13] Ono M. et al and the NSTX Team 2000 *Nucl. Fusion* **40** 557
- [14] Rice J. et al 2007 *Nucl. Fusion* **47** 1618
- [15] Solomon W.M., Kaye S.M., Bell R.E., LeBlanc B.P., Menard J.E., Rewoldt G. and Wang W. 2008 *Phys. Rev. Lett.* **101** 065004
- [16] Peeters A.G., Angioni C. and Strintzi D. 2007 *Phys. Rev. Lett.* **98** 265003
- [17] Hahn T.S., Diamond P.H., Gurcan O.D. and Rewoldt G. 2008 *Phys. Plasmas* **15** 055902
- [18] Linsker R. and Boozer A.H. 1982 *Phys. Fluids* **25** 143
- [19] Shaing K.C. 1983 *Phys. Fluids* **26** 3315
- [20] Solomon W.M. et al 2010 *Phys. Plasmas* **17** 056108
- [21] Shaing K.C. 2003 *Phys. Plasmas* **10** 1443
- [22] Park J.-K., Boozer A.H. and Menard J.E. 2009 *Phys. Rev. Lett.* **102** 065002
- [23] Gurcan O.D., Diamond P.H., Hahn T.S. and Singh R. 2007 *Phys. Plasmas* **14** 042306
- [24] Diamond P.H., McDevitt C.J. and Gurcan O.D. 2008 *Phys. Plasmas* **15** 012303
- [25] Diamond P.H., McDevitt C.J., Gurcan O.D., Hahn T.S., Wang W.X., Yoon E.S., Holod K., Lin Z., Naulin V. and Singh R. 2009 *Nucl. Fusion* **49** 045002
- [26] Camenen Y., Peeters A.G., Angioni C., Casson F.J., Hornsby W.A., Snodin A.P. and Strintzi D. 2009 *Phys. Rev. Lett.* **102** 125001
- [27] McDevitt C.J., Diamond P.H., Gurcan O.D. and Hahn T.S. 2008 *Phys. Plasmas* **16** 052302
- [28] Bell R.E., Andre R., Kaye S.M., Kolesnikov R.A., LeBlanc B.P., Rewoldt G., Wang W.X. and Sabbagh S.A. 2010 *Phys. Plasmas* **17** 082507
- [29] Hinton F.L. and Hazeltine R.D. 1976 *Rev. Mod. Phys.* **48** 239
- [30] Hirshman S.P. and Sigma D.J. 1981 *Nucl. Fusion* **21** 1079
- [31] Houlberg W.A., Shaing K.S., Hirshman S.P. and Zanstroff M.C. 1997 *Phys. Plasmas* **4** 3230
- [32] Marr K.D., Lipschultz B., Catto P.J., McDermott R.M., Reinke M.L. and Simakov A.N. 2010 *Plasma Phys. Control. Fusion* **52** 055010
- [33] Viezzer E. et al and the ASDEX Upgrade Team 2012 Investigations on the edge radial electric field at ASDEX upgrade *Proc. 39th EPS Conf. (Stockholm, Sweden, 2–6 July 2012)* <http://ocs.ciemat.es/epsicpp2012pap/pdf/O5.118.pdf>
- [34] Kagan G. and Catto P.J. 2010 *Phys. Rev. Lett.* **105** 045002
- [35] Grierson B.A., Burrell K.H., Heidbrink W.W., Lanctot M.J., Pablant N.A. and Solomon W.M. 2012 *Phys. Plasmas* **19** 056107
- [36] Wang W.X., Rewoldt G., Tang W.M., Hinton F.L., Manickam J., Zakharov L.E., White R.B. and Kaye S. 2006 *Phys. Plasmas* **13** 082501
- [37] Wang W.X., Diamond P.H., Hahn T.S., Ethier S., Rewoldt G. and Tang W.M. 2011 *Phys. Plasmas* **17** 072511
- [38] Rice J.E. et al 2011 *Phys. Rev. Lett.* **106** 215001
- [39] Wang W.X., Hahn T.S., Ethier S. and Zakharov L.E. 2011 *Phys. Rev. Lett.* **108** 085001
- [40] Kaye S.M., Solomon W.M., Bell R.E., LeBlanc B.P., Levinton F.M., Menard J.E., Rewoldt G., Sabbagh S.A., Wang W. and Yuh H. 2009 *Nucl. Fusion* **49** 045010

- [41] Kosuga Y., Diamond P.H. and Gurcan O.D. 2010 *Phys. Plasmas* **17** 102313
- [42] Menard J.E. *et al* and the NSTX Research Team 2010 *Nucl. Fusion* **50** 045008
- [43] Gerhardt S.P., Menard J.E., Park J.-K., Bell R., Gates D.A., LeBlanc B.P., Sabbagh S.A. and Yuh H. 2010 *Plasma Phys. Control. Fusion* **52** 104003
- [44] Park J.-K., Boozer A.H. and Glasser A.H. 2007 *Phys. Plasmas* **14** 052110
- [45] Park J.-K., Boozer A.H., Menard J.E., Garofalo A.M., Schaffer M.J., Hawryluk R.J., Kaye S.M., Gerhardt S.P., Sabbagh S.A. and the NSTX team 2009 *Phys. Plasmas* **16** 056115
- [46] Garofalo A.M. *et al* 2011 *Nucl. Fusion* **51** 083018
- [47] Burrell K.H., Garofalo A.M., Solomon W.M., Fenstermacher M.E., Osborne T.H., Park J.-K., Schaffer M.J. and Snyder P.B. 2012 *Phys. Plasmas* **19** 056117